Colloids and Surfaces B: Biointerfaces 128 (2015) 331–338

Contents lists available at ScienceDirect

Colloids and Surfaces B: Biointerfaces

journal homepage: www.elsevier.com/locate/colsurfb

Sulfisoxazole/cyclodextrin inclusion complex incorporated in electrospun hydroxypropyl cellulose nanofibers as drug delivery system

Zeynep Aytac[a,b], Huseyin Sener Sen[b], Engin Durgun[a,b], Tamer Uyar[a,b,*]

[a] Institute of Materials Science & Nanotechnology, Bilkent University, Ankara 06800, Turkey
[b] UNAM-National Nanotechnology Research Center, Bilkent University, Ankara 06800, Turkey

ARTICLE INFO

Article history:
Received 21 October 2014
Received in revised form 9 February 2015
Accepted 10 February 2015
Available online 17 February 2015

Keywords:
Electrospinning
Nanofibers
Hydroxypropyl cellulose
Cyclodextrin
Sulfisoxazole
Molecular modeling

ABSTRACT

Herein, hydroxypropyl-beta-cyclodextrin (HPβCD) inclusion complex (IC) of a hydrophobic drug, sulfisoxazole (SFS) was incorporated in hydroxypropyl cellulose (HPC) nanofibers (HPC/SFS/HPβCD-IC-NF) via electrospinning. SFS/HPβCD-IC was characterized by DSC to investigate the formation of inclusion complex and the stoichiometry of the complex was determined by Job's plot. Modeling studies were also performed on SFS/HPβCD-IC using *ab initio* technique. SEM images depicted the defect free uniform fibers and confirmed the incorporation of SFS/HPβCD-IC in nanofibers did not alter the fiber morphology. XRD analyses showed amorphous distribution of SFS/HPβCD-IC in the fiber mat. Release studies were performed in phosphate buffered saline (PBS). The results suggest higher amount of SFS released from HPC/SFS/HPβCD-IC-NF when compared to free SFS containing HPC nanofibers (HPC/SFS-NF). This was attributed to the increased solubility of SFS by inclusion complexation. Sandwich configurations were prepared by placing HPC/SFS/HPβCD-IC-NF between electrospun PCL nanofibrous mat (PCL-HPC/SFS/HPβCD-IC-NF). Consequently, PCL-HPC/SFS/HPβCD-IC-NF exhibited slower release of SFS as compared with HPC/SFS/HPβCD-IC-NF. This study may provide more efficient future strategies for developing delivery systems of hydrophobic drugs.

1. Introduction

Electrospinning is a well recognized and versatile technique for producing nanofibers from polymer solutions or polymer melts with the help of a very strong electric field [1]. Electrospun nanofibers and their nanofibrous mats are very good candidates for use in biotechnology, textiles, membranes/filters, scaffolds, composites, sensors due to their very high surface area to volume ratio, nanoporous structure and design flexibility for further functionalization [1,2]. Additionally, by given the morphological similarities between electrospun nanofibers and extracellular matrix, biomaterials for wound healing, drug delivery systems and scaffolds for tissue engineering could be developed through the electrospinning [1,2].

Certain hydroxyl groups of cellulose are substituted with another functional group yields its derivates. For example, hydroxypropyl cellulose (HPC) is a non-ionic cellulose derivative which can be synthesized by substituting with hydroxypropyl ether groups [3]. HPC could be used in the field of biomedical engineering for drug delivery applications [4,5]. Hence, electrospun HPC nanofibers also could be quite applicable in the area of biotechnology due to their distinctive characteristics as mentioned earlier. However, as far as we can ascertain, in the literature there are only few studies related to electrospinning of HPC [6–8]. Shukla et al. have produced electrospun HPC nanofibers from ethanol and 2-propanol solvent system [6]. In another study, Francis et al. have obtained HPC nanofibers in aqueous solution using polyethylene oxide as carrier matrix [7]. In the study of Periasamy et al. two types of enzymes were immobilized in HPC nanofibers [8].

Cyclodextrins (CDs) are a class of cyclic oligosaccharides (Fig. 1b) with several d-glucopyranoses linked by α-1,4-glycosidic bonds [9]. The most common native CDs have 6, 7, or 8 glucose units which are called as α-CD, β-CD and γ-CD, respectively [10]. There are also chemically modified CDs like hydroxypropyl-beta-cyclodextrin (HPβCD) in which some of the hydroxyl groups are substituted with hydroxypropyl groups. CDs are water-soluble molecules with rigid and well defined molecular structures. CDs take the shape of a truncated cone as shown in Fig. 1c [9]. As outstanding supramolecules

* Corresponding author. Tel.: +90 312 290 3571; fax: +90 312 266 4365.
E-mail addresses: tamer@unam.bilkent.edu.tr, tameruyar@gmail.com (T. Uyar).

http://dx.doi.org/10.1016/j.colsurfb.2015.02.019
0927-7765/

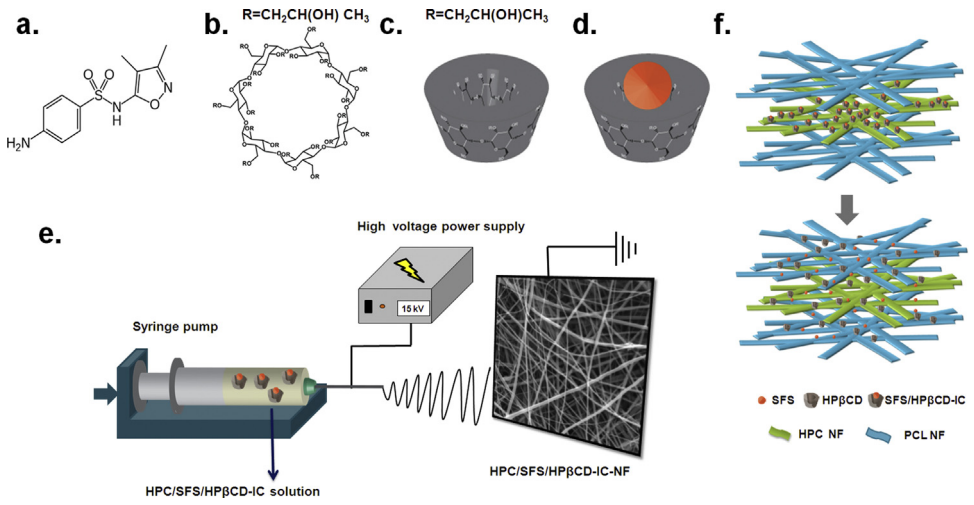

Fig. 1. Chemical structure of (a) sulfisoxazole, (b) HPβCD; schematic representation of (c) HPβCD, (d) SFS/HPβCD-IC, (e) electrospinning of nanofibers from HPC/SFS/HPβCD-IC solution, (f) the release of SFS from HPC/SFS/HPβCD-IC-NF.

with hydrophobic cavity, CDs are capable of forming non-covalent complexes with various compounds including poorly soluble drugs, antibiotics, and volatile compounds [9,10]. The inclusion complex (IC) formation in the CD systems is favored by substitution of the high-enthalpy water molecules within the CD cavity, with an appropriate guest molecule of low polarity [9]. Here, each guest molecule is enclosed within the hydrophobic cavity of the CD. CDs find applications in various fields such as pharmaceutical, cosmetic, food, chemical industries and agriculture [10]. For example, in food industry they can suppress unpleasant odors and tastes. On the other hand they can improve the solubility and provide protection against light or oxygen for guest compounds. Furthermore CDs can delay the degradation or evaporation of guest molecules that are highly volatile [10]. In the context of pharmaceutical industry, the solubility related problems of some drugs remain among the most challenging issues of the drug formulation, where CDs can enhance solubility, dissolution rate, chemical stability and bioavailability. Interestingly controlled release of poorly soluble drugs by means of CD-IC [9,10] is worth mentioning. In particular, a chemically modified CD like HPβCD is more suitable for the solubilization of hydrophobic drugs, because of its better aqueous solubility compared to native CDs [11]. It has been shown that CDs and CD-ICs can be used in functionalization of electrospun nanofibers for different applications like biomedical [12–17], filtration [18–20] and food packaging [21–26].

The sulfonamide drugs have a basic chemical structure comprising a sulfanilamide group and five or six-membered heterocyclic ring. Sulfisoxazole (SFS) (Fig. 1a) is a sulfonamide drug with an oxazole substituent. It is a weakly acidic in nature with antibiotic activity and poorly soluble in water [27]. The low solubility of SFS prevents its fast dissolution and leads to poor availability at the target site. Hence in this study, SFS was selected as a model drug for release experiments. There have been reports in the literature regarding CD-IC of SFS to evaluate chemical stability, thermal stability and solubility before and after complexation [28]. Another study deals with the characterization of IC via solubility, thermal and dissolution studies [29]. On the other hand, absorption and fluorescence spectra of sulpha drugs were analyzed in the presence of CD-IC to determine the stoichiometry of sulpha drugs and βCD [27].

In this study, HPC nanofibers incorporating SFS (HPC/SFS-NF) and IC of SFS with HPβCD (Fig. 1d) (HPC/SFS/HPβCD-IC-NF) were obtained via electrospinning for our drug delivery system (Fig. 1e). Since HPC nanofibers are water soluble, HPC/SFS-NF and HPC/SFS/HPβCD-IC-NF mats were sandwiched between electrospun polycaprolactone (PCL) nanofibrous mats (PCL-HPC/SFS-NF and PCL-HPC/SFS/HPβCD-IC-NF). PCL is a semi crystalline and hydrophobic polymer that is commonly used for biomedical applications such as tissue engineering scaffold [30] wound dressing [31] and drug delivery system [32], thanks to its biocompatibility and biodegradability. SFS/HPβCD-IC was characterized by DSC and continuous variation technique (Job's plot) in order to investigate the stoichiometry of the IC. In addition, inclusion complexation has been investigated by molecular modeling using *ab initio* techniques. HPC/SFS-NF and HPC/SFS/HPβCD-IC-NF were characterized by SEM, XRD and UV-Vis spectroscopy. Release studies were performed in phosphate buffered saline (PBS) (Fig. 1f) and quantified through HPLC. In addition, SFS (powder), HPC/SFS film, HPC/SFS/HPβCD-IC film; HPC/SFS-NF and HPC/SFS/HPβCD-IC-NF were also used as control samples for release studies.

2. Materials and methods

2.1. Materials

Hydroxypropyl cellulose (HPC, Mw ~ 300,000 g/mol, Scientific Polymer Products), polycaprolactone (PCL, Mn ~ 70,000–90000 g/mol, Sigma Aldrich), sulfisoxazole (SFS, min. 99%, Sigma Aldrich), hydroxypropyl-beta-cyclodextrin (HPβCD, average substitution degree per anhydroglucose unit 0.6, Wacker Chemie AG, Germany), ethanol (99.8%, Sigma Aldrich), dichloromethane (DCM, extra pure, Sigma Aldrich), N,N-dimethylformamide pestanal (DMF, Riedel), acetonitrile (ACN, chromasol, Sigma Aldrich), methanol (extra pure, Sigma Aldrich), potassium phosphate monobasic (Riedel de Haen), disodium hydrogen phosphate dodecahydrate (Riedel de Haen), sodium chloride (Sigma Aldrich) were purchased and used as received without any further purification. The water used in experiments was distilled – deionized from a Millipore Milli-Q ultrapure water system.

2.2. Preparation of solutions

Two types of SFS containing HPC nanofibers (HPC/SFS-NF and HPC/SFS/HPβCD-IC-NF) were prepared by incorporating 9% SFS (w/w, with respect to polymer). For producing HPC/SFS/HPβCD-IC-NF, the amount of SFS was determined as 1:1 molar ratio with HPβCD, and the same amount of SFS was used for HPC/SFS-NF. In order to prepare HPC/SFS-NF, SFS and 3% (w/v) HPC were

Table 1
The properties of the solutions used for electrospinning and morphological characteristics of the resulting electrospun nanofibers (the fiber size is reported as the average ± standard deviation and 100 fibers were analyzed for each case).

Solutions	% HPC[a] (w/v)	% HPβCD[b] (w/w)	% SFS[a] (w/w)	Viscosity (Pa s)	Conductivity (μS/cm)	Fiber diameter range (nm)	Fiber morphology
HPC	3	–	–	0.435	2.52	125 ± 50	Bead free nanofibers
HPC/SFS	3	–	9.11	0.673	4.13	90 ± 40	Bead free nanofibers
HPC/HPβCD/SFS-IC	3	50	9.11	0.551	13.04	60 ± 25	Bead free nanofibers

[a] With respect to solvent (ethanol).
[b] With respect to polymer (HPC).

dissolved in ethanol (HPC/SFS solution), stirred overnight at room temperature (RT) and subjected to electrospinning. With regard to SFS/HPβCD-IC containing HPC solution (HPC/SFS/HPβCD-IC solution), SFS was dissolved in ethanol at RT. Then 50% HPβCD (w/w, with respect to polymer) was added into the solution and stirred overnight at RT. Finally, 3% (w/v) HPC was added into the system, and dissolved for the electrospinning. For comparison, we have also electrospun HPC in ethanol (3%, w/v) without SFS or SFS/HPβCD-IC. Table 1 summarizes the compositions of the solutions used for the electrospinning of the nanofibers. To produce PCL nanofibers, 10% (w/v) PCL was dissolved in the binary solvent system containing DMF:DCM (v/v) (3:1).

2.3. Electrospinning of nanofibers and preparation of films

HPC, HPC/SFS, HPC/SFS/HPβCD-IC and PCL solutions were individually loaded into a 3 mL plastic syringe with needle diameter of 0.8 mm placed horizontally on the syringe pump (KD Scientific, KDS101). The flow rates of the polymer solutions were controlled by syringe pump to ensure homogeneous flow and fixed at 1 mL/h. The cylindrical metal collector was placed at a distance of 11 cm from the needle tip and covered by aluminum foil**.** The ground and the positive electrodes of the high voltage power supply (AU Series, Matsusada Precision Inc.) were clamped to the collector and the needle respectively. The electrospinning apparatus was enclosed in a Plexiglas box, and electrospinning was carried out at 16 kV, 22 °C and 20% relative humidity.

SFS containing HPC films (HPC/SFS film and HPC/SFS/HPβCD-IC film) were prepared by solution casting method using the same amounts of SFS, HPC and HPβCD. Note that the earlier described procedure was employed to prepare the various solutions for casting.

2.4. Characterization and measurements

In order to investigate the thermal properties of SFS-HPβCD-IC, powder of SFS-HPβCD-IC was obtained by evaporating the solvent. In addition, physical mixture of SFS and HPβCD (SFS-HPβCD-PM) was also prepared as control. The powders of SFS, HPβCD, SFS-HPβCD-PM and SFS-HPβCD-IC were analyzed with differential scanning calorimetry (DSC) (Netzsch, DSC 204F1). For DSC measurement, SFS, HPβCD, SFS-HPβCD-PM were prepared in an aluminum pan, held isothermally at 25 °C for 3 min and heated from 25 °C to 250 °C at a rate of 20 °C/min under nitrogen purge. SFS-HPβCD-IC was subjected to heating and cooling cycles consisting of: holding isothermally at 25 °C for 3 min, ramping from 25 °C to 250 °C at 20 °C/min, cooling at a rate of 20 °C/min down to 25 °C. It was subjected to a second cycle to investigate the change in thermal behavior following the first heat at a rate of 20 °C/min.

The stoichiometry of IC was investigated by the continuous variation technique (Job's plot) [33]. Equimolar (10^{-4} M) solutions of SFS and HPβCD prepared in ethanol were mixed to a standard volume varying the molar ratio (r, [SFS]/[SFS] + [HPβCD]) from 0 to 1 while keeping the total concentration of each solution constant. After stirring the solutions for 1 h at RT, the absorbance of the solutions was measured by UV–Vis spectroscopy (Varian, Cary 100). The diagram was plotted ΔAbs of SFS vs. r.

Anton Paar Physica MCR 301 rheometer was used to investigate the viscosity of HPC, HPC/SFS, HPC/SFS/HPβCD-IC and PCL solutions at RT. The rheometer was equipped with a cone/plate accessory (spindle type CP 40-2) at a constant shear rate of 100 sec^{-1}. The conductivity of solution was determined by Inolab® Multi 720-WTW at RT.

Scanning electron microscopy (SEM, FEI–Quanta 200 FEG) was used to examine the morphologies of the electrospun nanofibers. The samples were mounted on metal stubs using a double-sided adhesive tape and coated with Au/Pd layer (~6 nm) (PECS-682) to minimize the charging. Nearly 100 fibers were analyzed to calculate average fiber diameter (AFD).

The crystalline structure of the materials was examined with X-ray diffraction (XRD). XRD data for the powder of SFS and HPβCD; HPC NF, HPC/SFS-NF and HPC/SFS-HPβCD-IC NF mats were recorded using a PANalytical X'Pert powder diffractometer applying Cu Kα radiation in the 2θ range of 5–30°.

Since HPC is water-soluble, the sandwich configuration was prepared by placing the HPC/SFS/HPβCD-IC-NF between PCL nanofibrous mat for achieving the controllable release rate (PCL-HPC/SFS/HPβCD-IC-NF). The facile pressure is given by thumb forceps at open face of the membrane to wrap the structure. The same procedure was applied to prepare sandwich configuration of HPC/SFS-NF (PCL-HPC/SFS-NF). As control, the release of SFS (powder), HPC/SFS film, HPC/SFS/HPβCD-IC film, HPC/SFS-NF and HPC/SFS/HPβCD-IC-NF were also tested. A total immersion method was used to study the cumulative release profiles of SFS from the composite mats and control samples where the thickness of composite mats is ~400 μm (determined by Zeiss Axio Imager A2 m optical microscope). In this technique, each of the composite mats including 24 mg HPC/SFS-NF or 37 mg HPC/SFS/HPβCD-IC-NF and 30 mg PCL nanofibers and the control samples with same amount of SFS were immersed in 30 mL of phosphate buffered saline (PBS) medium at 37 °C at 50 rpm. At predetermined time intervals between 0 and 720 min, 0.5 mL of the test medium was withdrawn and an equal amount of the fresh medium was refilled. The released amount of SFS was determined by high performance liquid chromatography (HPLC, Agilient, 1200 series) equipped with VWD UV detector. The column was 2.1 mm × 50 mm, contained 3 μm packing (ACE, C8) and the detection was accomplished at 270 nm. Mobile phase, flow rate, injection volume and the total run time were 100% ACN, 0.1 mL/min, 20 μL and 4 min, respectively. The calibration samples were prepared in ethanol. According to predetermined calibration curve for SFS, the data were calculated to determine the cumulative amount of SFS released from the samples for each specified immersion period. The experiments were carried out in triplicate and the results were reported as average ± standard deviation.

In order to determine the actual loading (%) of SFS in nanofibers, a known weight of the sample was dissolved in ethanol and the amount of SFS in the sample was measured by HPLC in triplicate. According to calibration curve prepared in ethanol, the total amount of SFS in the sample and actual loading (%) was calculated.

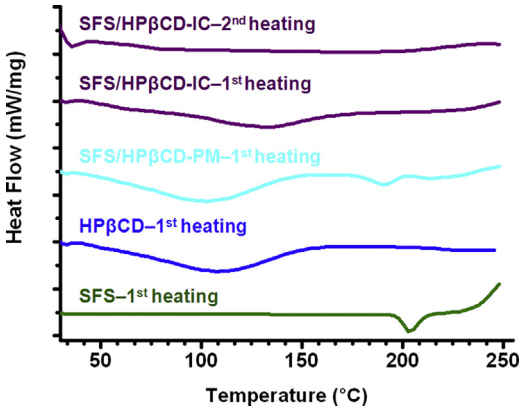

Fig. 2. DSC thermograms of first heating scan of SFS, HPβCD, SFS/HPβCD-PM, SFS/HPβCD-IC and second heating scan of SFS/HPβCD-IC.

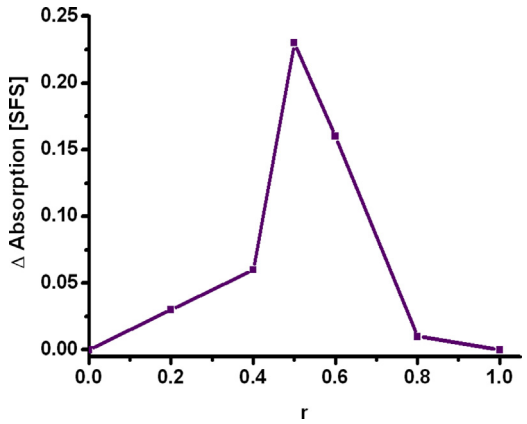

Fig. 3. Continuous variation plot (Job's plot) for the complexation of SFS with HPβCD obtained from absorption measurements.

The experiments were carried out in triplicate and the results were reported as average ± standard deviation.

To determine the solubility of SFS in each fiber, certain concentration of SFS (powder) (0.094 mM) and the same amount of SFS containing HPC/SFS/HPβCD-IC-NF were dissolved in water. For comparison, HPC/SFS-NF and HPC/SFS/HPβCD-IC-NF were scaled to the same weight. Lastly, UV absorbance of SFS in the samples was measured at 270 nm via UV–Vis–NIR spectroscopy (Varian, Cary 5000).

2.5. Computational method

The structures of SFS, pristine β-CD [34], HPβCD, and their ICs were optimized by using *ab initio* methods based on density functional theory (DFT) [35,36] implemented in the Vienna Ab initio simulation package [37,38]. The initial geometry of β-CD was obtained from Cambridge Structural Database [39]. HPβCD is constructed manually by adding four 2-hydroxypropyl groups on the primary groups of β-CD corresponding to a substitution degree per anhydroglucose unit of 0.6 which was compatible with the experiments [40]. The exchange-correlation was treated within Perdew-Burke-Ernzerhof parametrization of the generalized gradient approximation (GGA-PBE) [41] with inclusion of Van der Waals correction [42]. The element potentials were described by projector augmented-wave method (PAW) [43] using a plane-wave basis set with a kinetic energy cutoff of 400 eV. The Brillouin zone integration was performed at the Γ-point. All structures were considered as isolated molecules in vacuum and were relaxed using the blocked-Davidson algorithm with simultaneous minimization of the total energy and interatomic forces. The convergence on the total energy and force was tested and then set to 10^{-5} eV and 10^{-2} eV/Å, respectively.

3. Results and discussion

3.1. Thermal properties of SFS/HPβCD-IC

DSC thermograms of the powder of SFS, HPβCD, SFS-HPβCD-PM and SFS-HPβCD-IC are displayed in Fig. 2. The DSC curve of pure SFS exhibited a sharp endothermic peak at 203 °C (ΔH = 115.4 J/g) corresponding to the melting point of SFS [29]. The thermal transition of HPβCD ranged from 40 °C to 170 °C corresponding to dehydration of HPβCD-ring cavity, and appears as an endothermic transition with an enthalpy of 184.1 J/g. The endothermic transition of SFS was retained in SFS-HPβCD-PM (between 170 °C and 205 °C), and a broad endothermic transition corresponding to dehydration of HPβCD appeared in the range of 40 °C to 160 °C. The enthalpies of the above-mentioned transitions were 12.97 J/g and 169.2 J/g, respectively. These transitions observed in DSC thermogram of SFS-HPβCD-PM might be attributed to the presence of less or no interaction between SFS and HPβCD. When crystalline guest molecules form IC with CDs, the melting point either shifts or disappears in the DSC thermogram [29]. Notably, in DSC thermogram of SFS/HPβCD-IC the melting of SFS is not observed, however endothermic transitions between 40–80 °C and 80–190 °C were observed during the first heating scan. The disappearance of an endothermic peak of a guest molecule can be attributed to an amorphous state and/or to an inclusion complexation in which guest molecules being completely included into the cavity of CD by replacing water molecules. Moreover, no transition was observed in the second heating scan of SFS/HPβCD-IC. In the first heating scan of SFS/HPβCD-IC, the enthalpies of the endothermic transitions were 1.91 J/g and 58.78 J/g, respectively. Therefore, the enthalpies of transitions of SFS/HPβCD-IC were much smaller than those of SFS/HPβCD-PM. The enthalpy reduction also shows the interaction between SFS and CD in SFS/HPβCD-IC [44].

3.2. Stoichiometry determination by the continuous variation method (Job's plot)

The continuous variation method (Job's plot) was used to determine the stoichiometry of SFS/HPβCD-IC. According to this method, maximum point of the molar ratio (r) corresponds to the complexation stoichiometry. The plot in Fig. 3 shows the maximum at a molar ratio of about 0.5, indicating that the complexes were formed with 1:1 stoichiometry.

3.3. Molecular modeling of SFS/HPβCD-IC

The stability of CD-ICs when SFS included in HPβCD is examined by first-principles modeling techniques. Firstly, HPβCD is manually built by adding four 2-hydroxypropyl groups on the primary groups of pristine β-CD corresponding to a degree of substitution of 0.6. Various decoration patterns of substituents are considered (e.g. 1-2-3-4, 1-2-5-6, 1-3-5-7 where numbers indicate the relative position of substitution glucoses) [40,45]. The optimization results do not indicate any significant energy differences on the substituent pattern. On the other side the O-H interaction between substituents reduces the energy to some extent (up to 10 kcal/mol), thus hydroxypropyl (HP) arms may prefer to get closer as shown in Fig. 4b. Accordingly we consider 1-3-5-7 pattern as prototype and examine the possibility of IC formation. In order to form a complex, single SFS molecule is introduced into HPβCD at various positions. In addition, two different orientations are

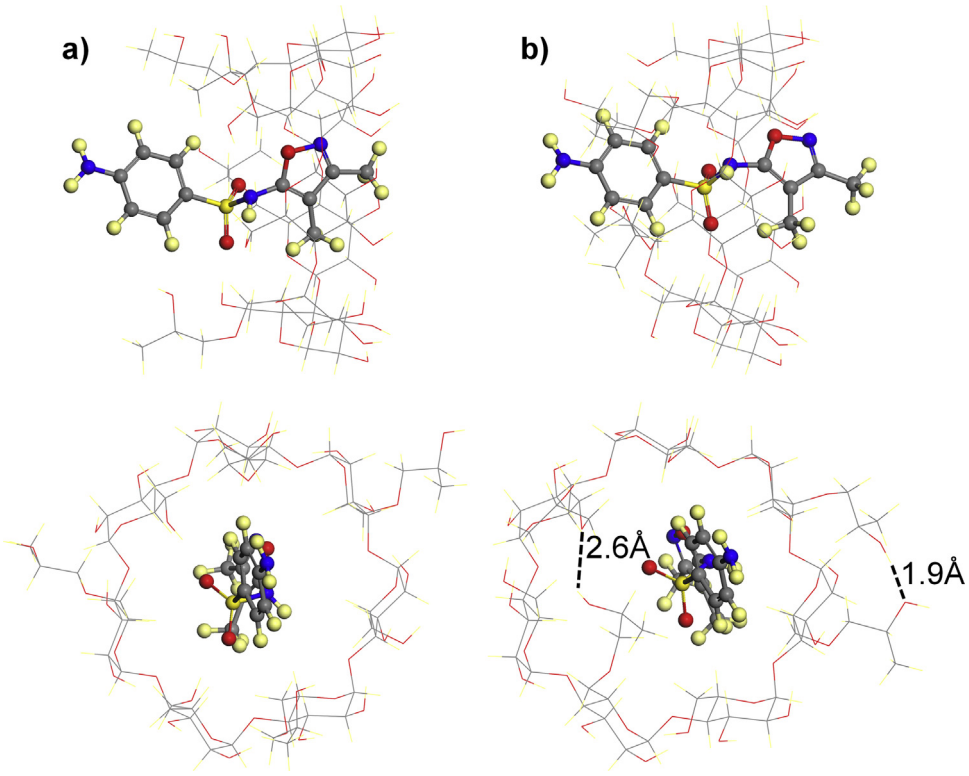

Fig. 4. Side and top view of optimized structures of SFS/HPβCD-IC when HP arms are (a) open and (b) close. Gray, red, and yellow spheres represent carbon, oxygen, and sulfur atoms, respectively. O—H bonding between HP groups are indicated by dashed lines. (For interpretation of the references to color in this figure legend, the reader is referred to the web version of this article.)

considered where NH_2- or CH_3-end points toward cavity. For each case the whole system is optimized without imposing any constraints. The lowest energy configurations are shown in Fig. 4. The complexation energy (E_{comp}) is calculated by

$$E_{comp} = E_{HP\beta CD} + E_{SFS} - E_{HP\beta CD+SFS}$$

where $E_{HP\beta CD}$, E_{SFS}, $E_{HP\beta CD+SFS}$ is the total energy (including van der Waals interaction) of HPβCD, SFS, and SFS/HPβCD-IC, respectively. E_{comp} is calculated as 35.05 and 32.49 kcal/mol for open and close HP arms, respectively. When HP arms get closer narrowing the rim, E_{comp} slightly reduces. Our results are in agreement with the Job's plot and support the formation of stable IC of SFS and HPβCD with 1:1 molar ratio.

3.4. Morphology of the nanofibers

Based on our preliminary experiments, ethanol was chosen as a solvent for dissolving both HPC and SFS. The concentration of HPC was determined as 3% (w/v) in ethanol to yield bead-free nanofibers. The amount of SFS (9%, w/w, with respect to HPC) was set at a 1:1 ratio with HPβCD in SFS/HPβCD-IC. Fig. 5 displays SEM images and AFD along with fiber diameter distributions of HPC NF, HPC/SFS-NF and HPC/SFS-HPβCD-IC NF. By optimizing the electrospinning parameters, we were able to obtain bead-free and uniform nanofibers from HPC, HPC/SFS and HPC/SFS-HPβCD-IC systems. The AFD of HPC NF was 125 ± 50 nm, whereas AFD of electrospun HPC/SFS-NF and HPC/SFS/HPβCD-IC-NF were 90 ± 40 nm and 60 ± 25 nm, respectively. The slight decrease in AFD could be explained by differences in conductivity and viscosity of HPC/SFS and HPC/SFS/HPβCD-IC solutions compared to HPC solution (Table 1). Stable jet formation usually depends on sufficiently high surface charge densities which are influenced by applied voltage and the electrical conductivity of the polymer solution. As the conductivity of a solution increases, the stretching increases due to the higher number of charges formed in the solution which thins the diameter of the fiber [46]. In addition, viscosity is important for the continuity of jet during electrospinning while lower viscosity leads to lower diameter nanofibers [47]. HPC/SFS and HPC/SFS/HPβCD-IC solutions have much higher conductivity and slightly higher viscosity than HPC solution; thereby AFD of HPC/SFS-NF and HPC/SFS/HPβCD-IC-NF were lower than HPC nanofibers. Moreover, HPC/SFS/HPβCD-IC-NF was thinner than HPC/SFS-NF possibly due to the higher conductivity and slightly lower viscosity of the parent solution.

Furthermore, we investigated the effect of SFS incorporation in the form of free SFS and SFS/HPβCD-IC on nanofiber morphology. Incorporation of SFS in HPC nanofibers did not deteriorate the shape and uniformity. Moreover relatively thinner fibers were obtained due to the higher conductivity of HPC/SFS and HPC/SFS/HPβCD-IC solutions. On the other hand, neither drug crystals nor aggregates were observed on the surfaces of nanofibers. Phase separation is not likely to occur as SFS is highly soluble in the HPC/ethanol system, while the solvent (ethanol) evaporates rapidly during electrospinning. For release experiments, sandwich-like composite mats were prepared in which the inner layer was HPC/SFS-NF or HPC/SFS/HPβCD-IC-NF mat and outer layers were electrospun PCL nanofibrous mat. SEM image and AFD (260 ± 110 nm) along with fiber diameter distributions of bead-free and smooth PCL nanofibers is shown in Fig. 5d.

3.5. Crystalline structure of nanofibers

XRD was performed to investigate the crystallinity of the samples. Fig. 6 represents the XRD patterns of the powder of SFS and HPβCD; HPC NF, HPC/SFS-NF and HPC/SFS-HPβCD-IC NF mats. XRD pattern of as received SFS indicated that SFS is a

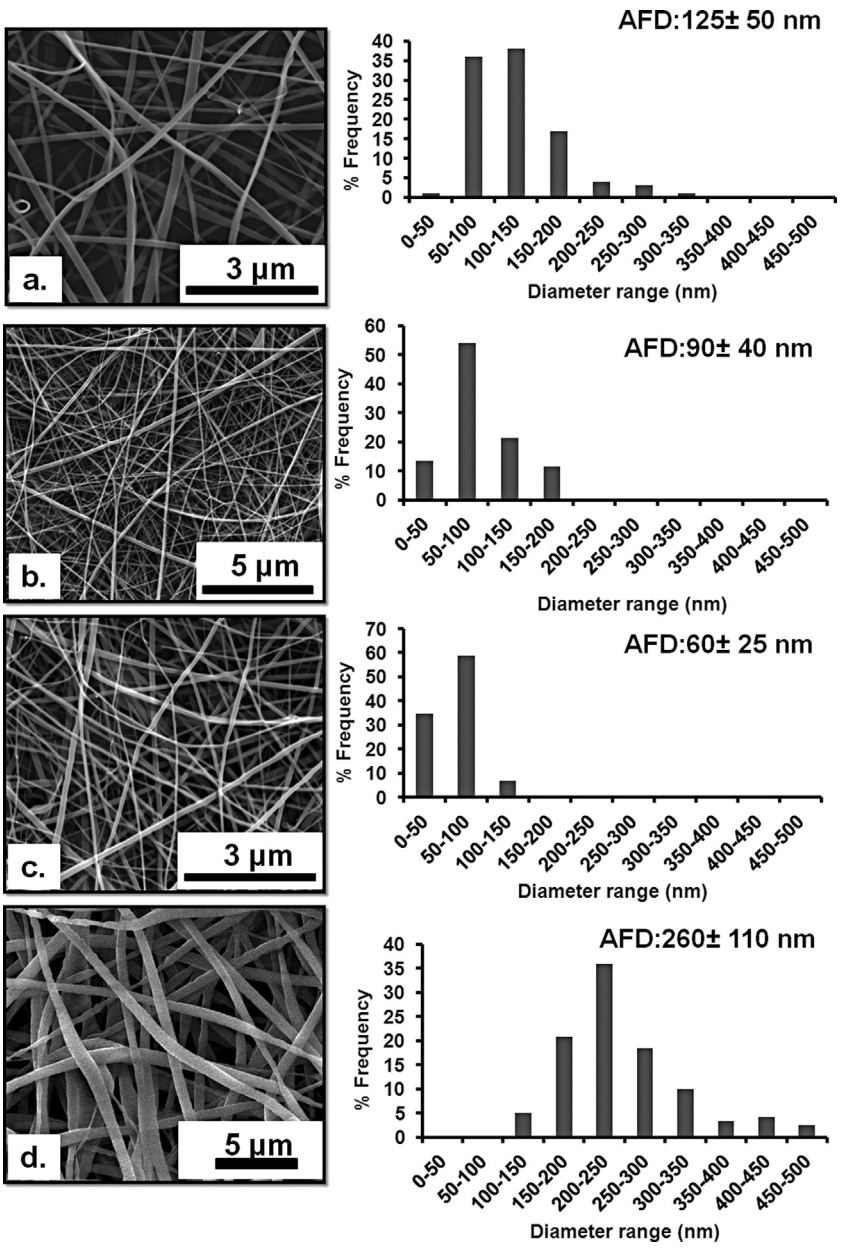

Fig. 5. SEM images and fiber diameter distributions with average fiber diameter (AFD) of the electrospun nanofibers obtained from solutions of (a) HPC, (b) HPC/SFS, (c) HPC/SFS/HPβCD-IC and (d) PCL.

crystalline material with characteristic diffraction peaks. The HPC NF diffraction exhibits a diffused pattern with two diffraction halos which show that the polymer is amorphous. In HPC/SFS-NF, the characteristic peaks of SFS were absent and only a hump of the amorphous form is noticed. This suggests that SFS was no longer in crystalline state; apparently it was converted into an amorphous state. In HPC/SFS ethanol solution, SFS is well solubilized and homogeneously distributed within the polymer solution, so during the electrospinning process, drug mobility is restricted due to the rapid evaporation of the solvent and the SFS molecules could not form crystalline aggregates. The absence of any intense and sharp peak in the pattern of HPβCD reveals that it possesses an amorphous structure. In the XRD pattern of HPC/SFS/HPβCD-IC-NF, the crystalline diffraction peak of SFS was also absent. That means SFS was in amorphous state in the HPC/SFS/HPβ CD-IC-NF [48].

3.6. In vitro release study

The cumulative release (%) of SFS from different samples is given in Fig. 7 as a function of immersion time. All samples depicted sustained release behavior of SFS over a period of 720 min (Fig. 7a). SFS followed a typical dual-stage release profile from all of the samples, an initial relatively fast release followed by a constant release. HPC/SFS/HPβCD-IC-NF released much more amount of SFS in total than SFS (powder) and HPC/SFS/HPβCD-IC film. This could be due to the high surface area of HPC/SFS/HPβCD-IC-NF compared to SFS (powder) and HPC/SFS/HPβCD-IC film. The actual loading (%) of SFS in HPC/SFS-NF and HPC/SFS/HPβCD-IC-NF were determined as 76 ± 1% and 73 ± 1%, respectively. However, total amount of released SFS was much higher from HPC/SFS/HPβCD-IC-NF than HPC/SFS-NF. Possible reason for this could be the higher surface area of HPC/SFS/HPβCD-IC-NF due to the lower fiber diameter as

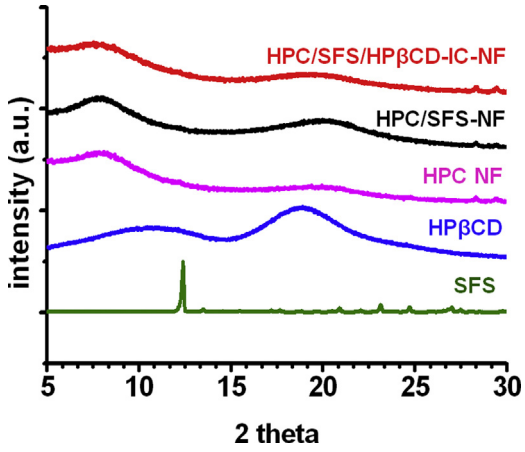

Fig. 6. XRD patterns of SFS, HPβCD, HPC NF and HPC nanofibers containing SFS.

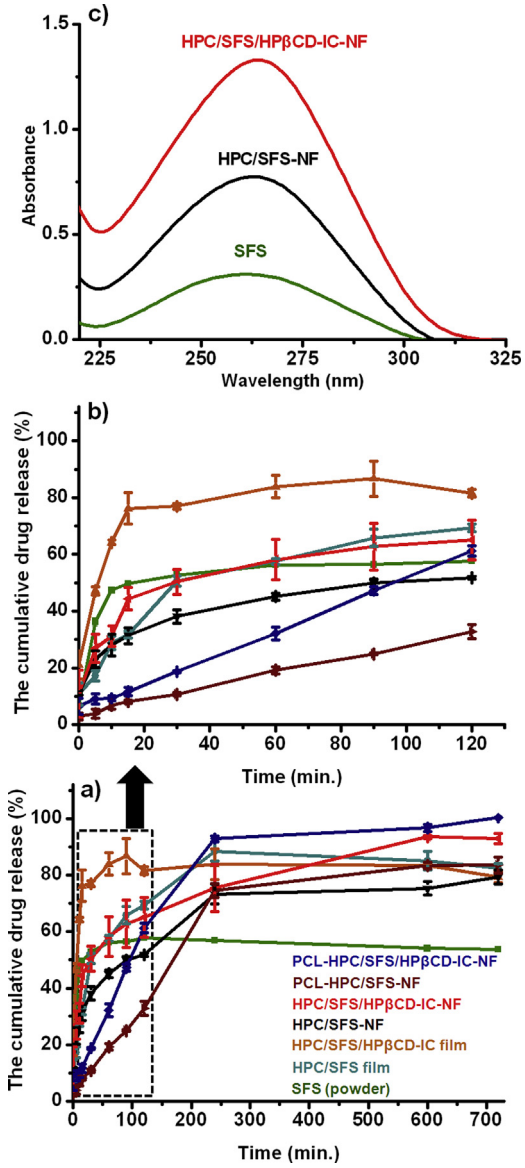

Fig. 7. The cumulative release of SFS from SFS (powder), HPC/SFS film, HPC/SFS/HPβCD-IC film, HPC/SFS-NF without PCL, HPC/SFS/HPβCD-IC-NF without PCL, PCL-HPC/SFS-NF and PCL-HPC/SFS/HPβCD-IC-NF for (a) 720 min, (b) 120 min ($n = 3$, the error bars in the figure represent the standard deviation (SD)), and (c) the solubility of SFS as powder, in HPC/SFS-NF and HPC/SFS/HPβCD-IC-NF in aqueous solution.

compared to HPC/SFS-NF and the presence of CD-IC that has higher solubility of SFS.

The release of SFS from powder sample was quite fast, thus the release reached to maximum (58%) in 120 min. Moreover, the release of SFS was faster from HPC/SFS/HPβCD-IC film than HPC/SFS/HPβCD-IC-NF initially, but over a longer immersion period, the release of SFS from HPC/SFS/HPβCD-IC film was slower (Fig. 7b). The initial fast release of SFS from HPC/SFS/HPβCD-IC film could be the location of SFS close to the surface in films due to the slow evaporation of the solvent during casting. On the other hand, high specific surface area of nanofibers provides higher accessibility for the drug to be in contact with the dissolution medium, thus accelerated drug-release. Moreover, the highly porous, three-dimensional structure of the nanofibrous mat can facilitate the dissolution of the drug in the medium and promote a rapid drug release [49]. In order to extend the release time of SFS from HPC/SFS-NF and HPC/SFS/HPβCD-IC-NF, we have prepared PCL-HPC/SFS-NF and PCL-HPC/SFS/HPβCD-IC-NF. SFS release from PCL-HPC/SFS-NF was slower compared to HPC/SFS-NF without PCL and PCL-HPC/SFS/HPβCD-IC-NF released SFS slower than HPC/SFS/HPβCD-IC-NF without PCL because of the presence of an extra layer for release of SFS. As a consequence, PCL-HPC/SFS/HPβCD-IC-NF exhibited a rapid release at the initial stage and then sustained release at the final stage. This might be crucial for many applications that are related with the prevention of bacteria proliferation. Bringing to the context, higher release at the initial stage is of great importance which limits the proliferation of bacteria in the beginning while sustained release inhibits the few bacteria which managed to proliferate [50].

HPC/SFS/HPβCD-IC-NF released higher amount of SFS in the initial stage and in each time period given on the graph; and the maximum amount of released SFS was almost 14% higher as compared to HPC/SFS-NF. As we mentioned before, this situation might be related with the existence of HPβCD in the matrix [51]. CDs have ability to enhance drug release from polymeric systems, since they increase the concentration of diffusible species within the matrix [52]. When a hydrophobic drug makes complex with CD its solubility increases considerably where CD-IC is usually more hydrophilic than the free drug. The nanofibers containing CD-IC wet easier and the structure disintegrates dissolving the substance quickly [51,53]. The enhancement in the solubility of SFS with HPC/SFS/HPβCD-IC-NF was verified by solubility test. The UV–Vis spectroscopy of SFS (powder), HPC/SFS-NF and HPC/SFS/HPβCD-IC-NF dissolved in water is shown in Fig. 7c. HPC/SFS-NF allows the SFS drug to be dispersed in the medium which facilitates its dissolution. Although same amount of SFS was used for each sample the solubility of SFS has increased much more in HPC/SFS/HPβCD-IC-NF. Additionally, the presence of CD may lower the required dose of an active molecule by improving its solubility. Consequently, HPC/SFS/HPβCD-IC-NF could be used as an efficient drug delivery system for wound dressing purpose.

4. Conclusion

The concept of employing electrospun nanofibers as matrix and improving the solubility of hydrophobic compounds by CD-ICs are well-known approaches those have been investigated. Therefore, we have anticipated that combination of drug/CD-IC and versatile electrospinning process could enable HPC nanofibers to be used for the delivery of a variety of hydrophobic drugs. Here, SFS was used as a model drug to study its release kinetics from electrospun HPC nanofibers incorporating SFS/HPβCD-IC. The stoichiometry of the complex between SFS and HPβCD was determined to be 1:1 by Job's plot. Furthermore, modeling studies performed using *ab initio* techniques also revealed that the

stoichiometry of the SFS/HPβCD-IC was 1:1 (SFS:HPβCD). Therefore, the results of molecular modeling are in good agreement with the experimental data. SFS release from PCL-HPC/SFS/HPβCD-IC-NF that was prepared by placing HPC/SFS/HPβCD-IC-NF between PCL nanofibrous mats was slower compared to HPC/SFS/HPβCD-IC-NF without PCL. Controlled release of SFS was attained from HPC/SFS-NF and HPC/SFS-HPβCD-IC NF for a period of 720 min, yet we observed that higher amount of SFS was released from HPC/SFS-HPβCD-IC-NF when compared to HPC/SFS-NF. This is possibly due to the property of CD-IC to enhance the solubility of hydrophobic SFS molecules via inclusion complexation with HPβCD and higher surface area of HPC/SFS/HPβCD-IC-NF compared to HPC/SFS-NF. As a result, PCL-HPC/SFS/HPβCD-IC-NF depicted slow release and highest amount of total SFS release. This study contributes to the existing literature for improving CD-IC functionalized electrospun nanofibers that might be used as wound dressing with characteristics of both CD and electrospun nanofibers for delivery of poorly soluble drugs.

Acknowledgments

Dr. Uyar acknowledges The Scientific and Technological Research Council of Turkey (TUBITAK) -Turkey (Project no. 111M459) and EU FP7-PEOPLE-2009-RG Marie Curie-IRG (NANOWEB, PIRG06-GA-2009-256428) and The Turkish Academy of Sciences – Outstanding Young Scientists Award Program (TUBA-GEBIP) -Turkey for partial funding of the research. Z. Aytac thanks to TUBITAK (Project no. 111M459 and 213M185) for the PhD scholarship.

References

[1] J.H. Wendorff, S. Agarwal, A. Greiner, Electrospinning: Materials, Processing, and Applications, John Wiley & Sons Publishing, Weinheim, 2012.
[2] A. Greiner, J.H. Wendorff, Angew. Chem. Int. Ed. 46 (2007) 5670.
[3] J.H. Guo, G.W. Skinner, W.W. Harcum, P.E. Barnum, Pharm. Sci. Technol. Today 1 (1998) 254.
[4] A. Abdelbary, A.H. Elshafeey, G. Zidan, Carbohydr. Polym. 77 (2009) 799.
[5] Y. Bai, Z. Zhang, A. Zhang, L. Chen, C. He, X. Zhuang, X. Chen, Carbohydr. Polym. 89 (2012) 1207.
[6] S. Shukla, E. Brinley, H.J. Cho, S. Seal, Polymer 46 (2005) 12130.
[7] L. Francis, A. Balakrishnan, K. Sanosh, E. Marsano, Mat. Lett. 64 (2010) 1806.
[8] V. Periasamy, K. Devarayan, M. Hachisu, J. Fiber Bioeng. Inform. 5 (2012) 191.
[9] J. Szejtli, Chem. Rev. 98 (1998) 1743.
[10] E.M.M. Del Valle, Process Biochem. 39 (2004) 1033.
[11] L. Szente, J. Szejtli, Adv. Drug Deliv. Rev. 36 (1999) 17.
[12] M.F. Canbolat, A. Celebioglu, T. Uyar, Colloids Surf. B: Biointerfaces 115 (2014) 15.
[13] A. Celebioglu, O.C.O. Umu, T. Tekinay, T. Uyar, Colloids Surf. B: Biointerfaces 116 (2014) 612.
[14] X.Z. Sun, G.R. Williams, X.X. Hou, L.M. Zhu, Carbohydr. Polym. 94 (2013) 147.
[15] T. Vigh, T. Horváthová, A. Balogh, P.L. Sóti, G. Drávavölgyi, Z.K. Nagy, G. Marosi, Eur. J. Pharm. Sci. 49 (2013) 595.
[16] X. Luo, C. Xie, H. Wang, C. Liu, S. Yan, X. Li, Int. J. Pharm. 425 (2012) 19.
[17] J.L. Manasco, C. Tang, N.A. Burns, C.D. Saquing, S.A. Khan, RSC Adv. 4 (2014) 13274.
[18] T. Uyar, R. Havelund, J. Hacaloglu, F. Besenbacher, P. Kingshott, ACS Nano 4 (2010) 5121.
[19] T. Uyar, R. Havelund, Y. Nur, A. Balan, J. Hacaloglu, L. Toppare, F. Besenbacher, P. Kingshott, J. Membr. Sci. 365 (2010) 409.
[20] T. Uyar, R. Havelund, Y. Nur, J. Hacaloglu, F. Besenbacher, P. Kingshott, J. Membr. Sci. 332 (2009) 129.
[21] F. Kayaci, Y. Ertas, T. Uyar, J. Agric. Food Chem. 61 (2013) 8156.
[22] F. Kayaci, O.C.O. Umu, T. Tekinay, T. Uyar, J. Agric. Food Chem. 61 (2013) 3901.
[23] F. Kayaci, T. Uyar, Carbohydr. Polym. 90 (2012) 558.
[24] F. Kayaci, T. Uyar, Food Chem. 133 (2012) 641.
[25] E. Mascheroni, C.A. Fuenmayor, M.S. Cosio, G.D. Silvestro, L. Piergiovanni, S. Mannino, A. Schiraldi, Carbohydr. Polym. 98 (2013) 17.
[26] Z. Aytac, S.Y. Dogan, T. Tekinay, T. Uyar, Colloids Surf. B: Biointerfaces 120 (2014) 125.
[27] A.A.M. Prabhu, G. Venkatesh, N. Rajendiran, J. Solut. Chem. 39 (2010) 1061.
[28] B. Szafran, J. Pawlaczyk, J. Incl. Phenom. Mol. Recognit. Chem. 23 (1996) 277.
[29] G. Gladys, G. Claudia, L. Marcela, Eur. J. Pharm. Sci. 20 (2003) 285.
[30] L.G. Mobarakeh, M.P. Prabhakaran, M. Morshed, M.H. Nasr-Esfahani, S. Ramakrishna, Biomaterials 29 (2008) 4532.
[31] E.J. Chong, T.T. Phan, I.J. Lim, Y.Z. Zhang, B.H. Bay, S. Ramakrishna, C.T. Lim, Acta Biomat. 3 (2007) 321.
[32] M. Zamani, M. Morshed, J. Varshosaz, M. Jannesari, Eur. J. Pharm. Biopharm. 75 (2010) 179.
[33] P. Job, Ann. di Chim. Appl. 9 (1928) 113.
[34] K. Lindner, W. Saenger, Carbohydr. Res. 99 (1982) 103.
[35] W. Kohn, L.J. Sham, Phys. Rev. 140 (1965) A1133.
[36] P. Hohenberg, W. Kohn, Phys. Rev. 136 (1964) B864.
[37] G. Kresse, J. Furthmüller, Phys. Rev. B 54 (1996) 11169.
[38] G. Kresse, J. Furthmüller, Comput. Mat. Sci. 6 (1996) 15.
[39] F.H. Allen, Acta Crystallogr. Sect. B: Struct. Sci. 58 (2002) 380.
[40] P. Mura, G. Bettinetti, F. Melani, A. Manderioli, Eur. J. Pharm. Sci. 3 (1995) 347.
[41] J.P. Perdew, J.A. Chevary, S.H. Vosko, K.A. Jackson, Phys. Rev. B 46 (1992) 6671.
[42] S. Grimme, J. Comput. Chem. 27 (2006) 1787.
[43] P.E. Blöchl, Phys. Rev. B 50 (1994) 17953.
[44] M.O. Ahmed, I. El-Gibaly, S.M. Ahmed, Int. J. Pharm. 171 (1998) 111.
[45] T. Irie, K. Fukunaga, A. Yoshida, K. Uekama, H.M. Fales, J. Pitha, Pharm. Res. 5 (1988) 713.
[46] T. Uyar, F. Besenbacher, Polymer 49 (2008) 5336.
[47] S. Ramakrishna, An Introduction to Electrospinning and Nanofibers, World Scientific Publishing Company Incorporated, Singapore, 2005.
[48] E.E.M. Eid, A.B. Abdul, F.E.O. Suliman, M.A. Sukari, A. Rasedee, S.S. Fatah, Carbohydr. Polym. 83 (2011) 1707.
[49] X. Li, M.A. Kanjwal, L. Lin, I.S. Chronakis, Colloids Surf. B: Biointerfaces 103 (2013) 182.
[50] K. Kim, Y.K. Luu, C. Chang, D. Fang, B.S. Hsiao, B. Chu, M. Hadjiargyrou, J. Control. Release 98 (2004) 47.
[51] J. Szejtli, Cyclodextrin Technology, Kluwer academic, Dordrecht, 1988.
[52] D.C. Bibby, N.M. Davies, I.G. Tucker, Int. J. Pharm. 197 (2000) 1.
[53] J. Panichpakdee, P. Supaphol, Carbohydr. Polym. 85 (2011) 251.